

# BEAM DYNAMICS STUDIES FOR MULTI-GeV PROTON AND H-MINUS LINACS\*

J.-P. Carneiro<sup>†</sup> Fermi National Accelerator Laboratory, IL 60510, U.S.A.,  
 B. Mustapha, P. N. Ostroumov, Argonne National Laboratory, Argonne, IL 60439, U.S.A.

## Abstract

Significant advances were demonstrated in the design and computer simulations of multi-GeV proton and H-minus linacs. Several codes were applied for the simulation of the 8 GeV linac and resulted to extremely good coincidence of all beam parameters. New procedures such as stripping of H-minus ions due to various mechanisms were implemented into the tracking code TRACK.

## INTRODUCTION

High-intensity proton and H<sup>-</sup> linacs are being developed for applications such as spallation neutron sources, production of radioactive ion beams, transmutation of nuclear waste or neutrino physics. These proton drivers can deliver up to multi-MW beams in either CW or pulsed mode.

This paper presents general considerations for the design of high-intensity proton and H<sup>-</sup> linacs. After describing some high-intensity linacs under design or operation worldwide, we overview the importance of limiting the beam losses in these linacs to 1 W/m. A description of the design considerations at first zero current and then high-current follows with simulations performed by the codes TRACK [1] and ASTRA [2] for the FNAL 8-GeV superconducting pulsed linac. The impact of beam-line element misalignments and jitters is also presented together with the steering correction algorithm implemented in TRACK. Finally an overview of the H<sup>-</sup> stripping effects from blackbody radiation, residual gas and magnetic fields is described.

## MULTI-GeV PROTON AND H<sup>-</sup> LINACS

Table 1 presents an overview of the multi-GeV proton and H<sup>-</sup> linacs currently in consideration or operation worldwide. Typical front-end for these linacs are made of normal-conducting structures (like Drift Tube Linacs and Coupled Cavity Linacs) with a transition to superconducting linacs at high-energy: 50 MeV for the European Spallation Source (ESS, [3]), 160 MeV for the CERN Superconducting Proton Linac (SPL [4]) or 185 MeV for the Spallation Neutron Source (SNS [5]). A different approach has been taken at Fermilab in the design of 8-GeV pulsed

Table 1: Overview of High-intensity Linacs under Design or in Operation

Project	E [GeV]	I <sub>av</sub> [mA]	Power [MW]	Status
FNAL 8-GeV Pulsed	8	25	2	proposed
FNAL 3-GeV CW	3	1	3	proposed
CERN HP-SPL	5	40	>4	proposed
ESS (EU)	2.5	75	5	proposed
ORNL SNS1	1	26	1.4	in oper.
ORNL SNS2	1.3	42	3	proposed

linac [6]. Taking advantage of the development and excellent performance of Spoke Cavities, it was decided to accelerate the beam from  $\sim 10$  MeV to 420 MeV with two types of superconducting Single Spoke Resonators (SSR 1) and (SSR 2) and one type of superconducting Triple Spoke Resonators (TSR). To boost the beam from  $\sim 2.5$  MeV to  $\sim 10$  MeV it was decided to use 16 room temperature cross-bar H-type (CH) cavities. For the current version of the FNAL Proton Driver, i.e the 3-GeV CW linac, these cross-bar cavities has been replaced by Single Spoke Resonators [7] making the transition to superconducting section at  $\sim 2.5$  MeV.

## THE 1 W/M LOSS CRITERIA

The most challenging requirement in the design of a high power H<sup>-</sup> linac is to minimize beam loss and be able to perform timely “hands-on maintenance” on the accelerator when needed. This requirement implies an activation limit below 100 mrem/hr at 30 cm from the component surface, after extended operation of the machine ( $\sim 100$  days) and four hours of down time [8]. Simulations and measurements for operating facilities such as the Los Alamos Neutron Science Center (LANSCE) 800 MeV proton and H<sup>-</sup> linac and Proton Accumulator Ring indicate this criterion corresponds to a beam power loss of about 1 W/m or less for energies above 100 MeV. For lower energies higher losses may be tolerated since the activation is less effective.

Figure 1 shows the permissible beam loss per unit length to achieve 0.1 W/m as a function of the beam kinetic energy along the FNAL 8 GeV pulsed and 3 GeV CW linacs and the SNS linac. At the final energy, losses should not exceed  $\sim 10^{-7}$  m<sup>-1</sup> for these linacs operating at full power.

\* Work supported by the U.S. Department of Energy under Contracts DE-AC02-06CH11357 and DE-AC02-07CH11359.

<sup>†</sup> carneiro@fnal.gov

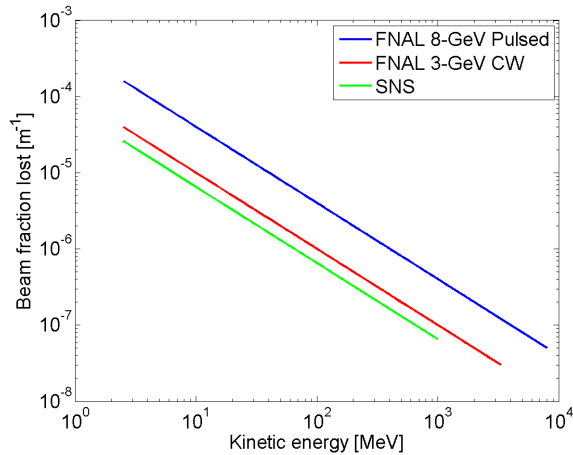


Figure 1: Permissible beam loss fraction as a function of the beam kinetic energy to achieve 0.1 W/m for the FNAL 8-GeV pulsed linac operating at 2 MW, the FNAL 3-GeV CW linac operating at 3 MW and the SNS linac operating at 1.4 MW.

## BEAM DYNAMICS

The general design requirements for a high intensity proton linac that need to be fulfilled in order to avoid RMS emittance growth and minimize beam losses are reported in Ref. [9] and summarized thereafter. All the requirements need to be taken into account in the design of the linac, especially in its front end, in order to control the growth of beam halo that would lead to particle losses and radio-activation of beam line components.

The design of the FNAL Proton Driver described in Fig. 2 is taken as an example to illustrate these rules. The FNAL 8-GeV linac was designed to deliver  $1.56 \times 10^{14}$  protons to the Main Injector in typical pulse length of 1 ms leading to an average beam current of 25 mA per pulse and a peak beam current of 45 mA.

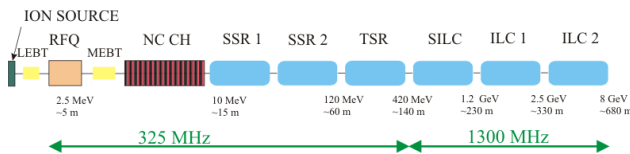


Figure 2: Schematic layout of the FNAL 8-GeV superconducting pulsed linac.

### Zero Current Design Considerations

- The zero current phase advance of transverse and longitudinal oscillations should be kept below  $90^\circ$  per focusing period to avoid parametrically-excited instabilities at high current.
- The transverse and longitudinal wavenumbers  $k_{T0}$ ,  $k_{L0}$  must change adiabatically along the linac. This feature minimizes the potential for mismatches and

helps ensure a current independent lattice. The wavenumbers of particle oscillations are expressed as:

$$k_{T0} = \frac{\sigma_{T0}}{L_f}, \quad k_{L0} = \frac{\sigma_{L0}}{L_f} \quad (1)$$

where  $\sigma_{T0}$  and  $\sigma_{L0}$  are the zero current transverse and longitudinal phase advances per focusing period of length  $L_f$ .

- Avoid the  $n = 1$  parametric resonance between the transverse and longitudinal motion. The condition for occurrence of an  $n$ -th order transverse motion parametric resonance is:

$$\sigma_{T0} = \frac{n}{2} \sigma_{L0} \quad (2)$$

The strongest resonance is for  $n = 1$  and can occur particularly in superconducting linacs due to the availability of high accelerating gradients and relatively long focusing periods. These instabilities can be avoided by proper choice of operational tunes in the Kapchinskiy diagram.

### High-Current Design Considerations

- Avoid energy exchange between the transverse and longitudinal planes via space-charge resonances, either by providing beam equipartitioning or by avoiding instable areas in Hofmann's stability charts.
- Provide proper matching in the lattice transitions to avoid appreciable halo formation.
- Keep ratio aperture-to-RMS-beam-size  $> 10$ .

Simulations with TRACK and ASTRA of the FNAL Proton Driver at zero current and 45 mA are presented in Fig. 3.

The transverse and longitudinal phase advances per focusing periods ( $\sigma_{T0}$ ,  $\sigma_{L0}$ ) depicted in Fig. 3(a) present some strong but innocuous jumps due to the changing length of the focusing periods at transitions between different types of cavities. Aside from few periods the transverse and longitudinal phase advances are kept below  $90^\circ$ . The smooth evolution of the transverse and longitudinal wavenumbers defined in Equation 1 ( $k_{T0}$ ,  $k_{L0}$ ) are shown in Fig. 3(b). This design requirement is achieved by properly selecting the length of the focusing periods and adequately adjusting the synchronous phase of each cavity.

The Kapchinskiy diagram presented in Fig. 3(c) shows the evolution of  $\cos(\sigma_{T0})$  as a function of the defocusing factor  $\gamma_s$  for each one of the 110 periods of the linac. The defocusing factor is defined as:

$$\gamma_s = \frac{\pi}{2} \frac{1}{(\beta\gamma)^3} \frac{L_f^2}{\lambda} \frac{eE_m \sin(\phi_s)}{m_0 c^2} \quad (3)$$

where  $m_0 c^2$  is the particle rest mass,  $\beta$  is the particle relative velocity,  $\gamma$  is the Lorentz factor,  $\lambda$  is the wavelength

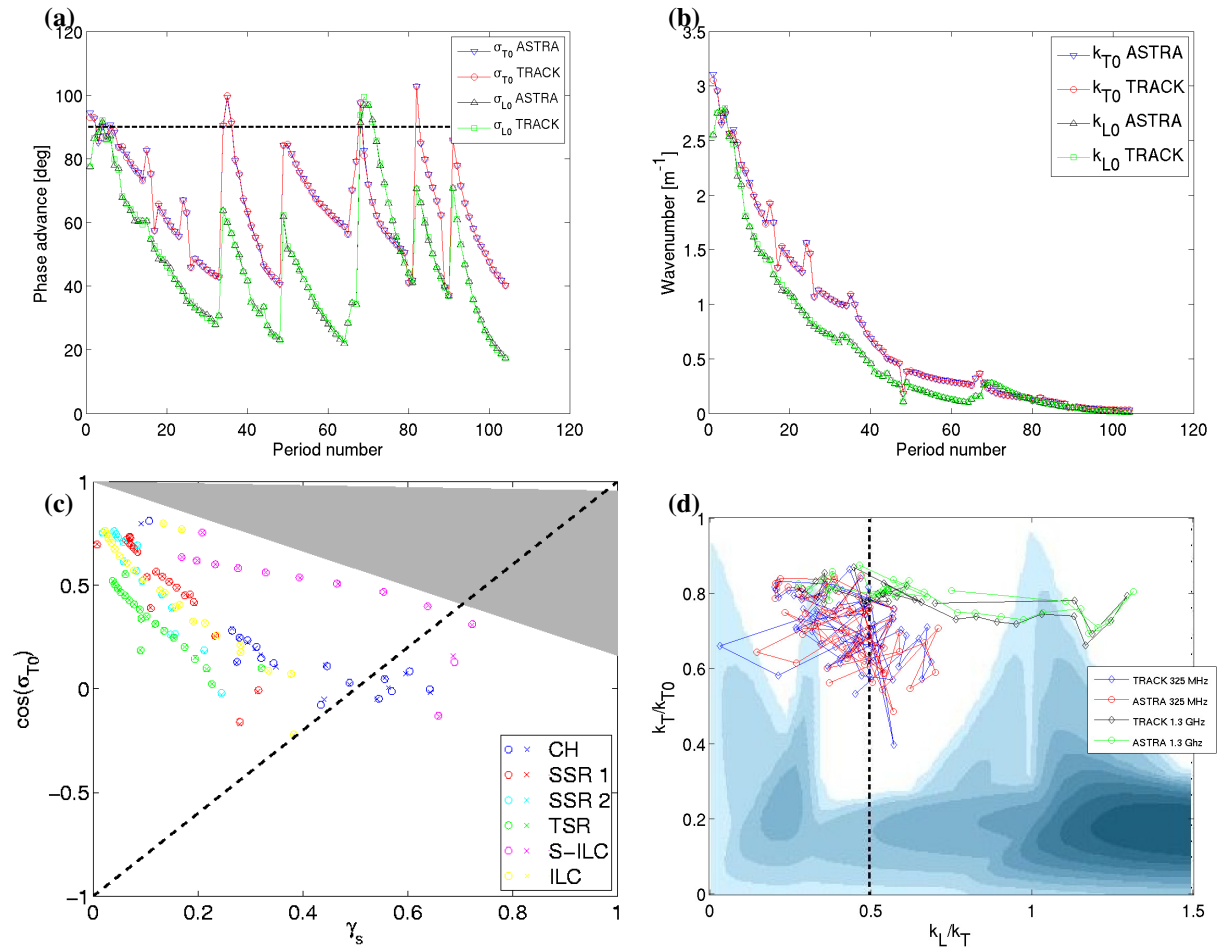


Figure 3: (a) Phase advance and (b) wavenumber per linac focusing period at zero-current and (c) Kapchinskiy and (d) Hofmann stability charts. Simulations performed with TRACK and ASTRA for the FNAL 8-GeV pulsed linac at 43.25 mA. The circles in the Kapchinsky chart represent TRACK and crosses ASTRA.

of the RF field,  $L_f$  is the length of the focusing period,  $E_m$  is the amplitude of the equivalent traveling wave of the accelerating field and  $\phi_s$  is the synchronous phase. The gray area in Fig. 3(c) shows the boundary for the  $n = 1$  parametric resonance (as defined in Eq. 2) to occur. The dashed line corresponds to the stable region for the phase motion near the separatrix boundary at a phase angle of  $-2|\phi_s|$ . The Kapchinskiy diagram requires the defocusing factor  $\gamma_s$  to be kept below  $\sim 0.7$  to insure the stability for all particles. As depicted in Fig. 3(c), the majority of the operating tunes are located in stable regions with few points lying on unstable ones. These tune points correspond to matching sections and are not expected to affect the beam since the susceptibility to instability exists for only a short distance compared to the betatron oscillation wavelength.

An important parameter to monitor in the design of a high intensity accelerator is the tune depression  $\eta$  defined as:

$$\eta = \frac{k}{k_0} \quad (4)$$

where  $k$  is the wavenumber per focusing period depressed by the space-charge and  $k_0$  the same parameter without space-charge. The tune depression evaluates the importance of the space-charge force in the focusing channel. In fact, high intensity beams in linacs are subject to tune depression which even if it's modest ( $0.5 < k/k_0 < 1.0$ ) still provide a large spread of individual particles tunes which is likely to induce parametric resonances. The dominant parametric resonance is the 2:1 which is caused by envelope mismatch and it is the main mechanism of halo formation. Reference [9] reports a moderate transverse and longitudinal tune depression along the linac ( $0.5 < \eta_{T,L} < 0.8$ ).

The tune depression is not only a useful tool to quantify the parametric resonances between single particles and the core of the beam, it also gives information about the coherent resonances of the core of the beam with itself called the core-core resonances. A commonly used tool in the study of core-core resonances is the Hofmann's chart which indicates, for a given longitudinal to transverse emittance ratio, regions sufficiently large to ensure stable operation of

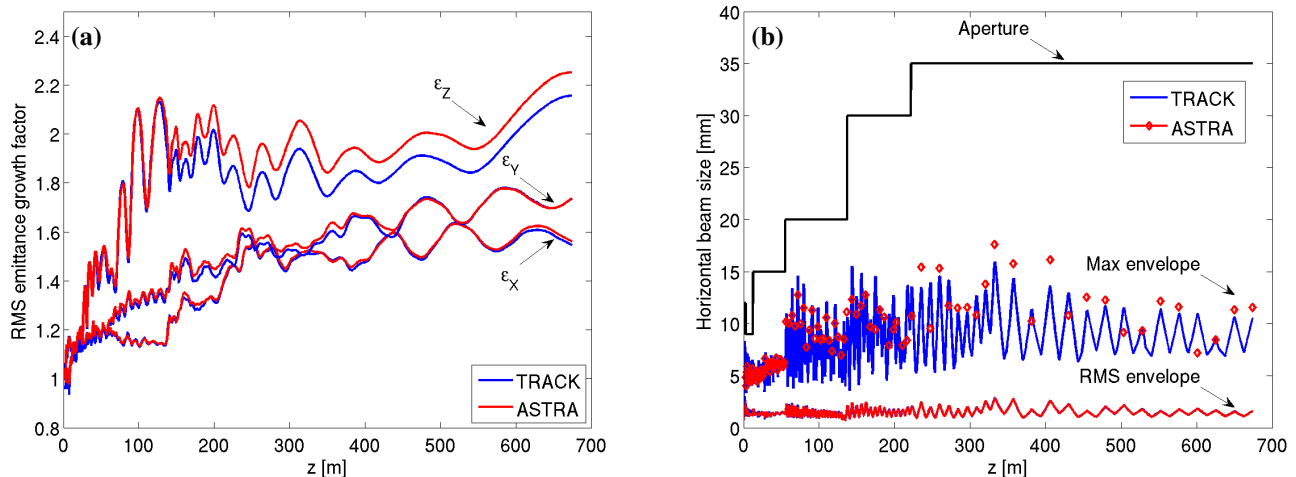


Figure 4: TRACK and ASTRA simulations of (a) the RMS normalized emittance and (b) RMS and maximum beam envelope for the FNAL 8-GeV pulsed linac at 43.25 mA, from the RFQ to the last accelerating cavity ( $z \simeq 674$  m).

non-equipartitioned beams. Figure 3(d) presents the Hofmann's stability chart for a longitudinal to transverse emittance ratio of  $\epsilon_L/\epsilon_T = 2$  which characterizes the FNAL Proton Driver at the design current of 45 mA. The horizontal axis on the chart is the ratio between the transverse and longitudinal tune depression and the vertical axis is the tune depression. The shaded areas indicate regions where non-equipartitioned beams are subject to space-charge coupling resonances that are expected to cause emittance transfer between transverse and longitudinal planes (the degree of shading indicates the speed of the process). The vertical dashed line shows the condition for equipartition. The dangerous resonance in the chart is the fourth order even mode one located at around a tune ratio of 1. The peaks on the left part of the chart represent weak coupling resonances that would take a long time to develop. As observed in Figure 3(d) the operating tunes computed with TRACK and ASTRA lie in stable (white) areas which points out that core-core resonances are not a concern for the current design of the FNAL Proton Driver.

Figure 4 presents the tracking performed by TRACK and ASTRA of the 45 mA distribution along the FNAL 8-GeV linac. The transverse and longitudinal RMS emittance growth factor shown in Fig. 4(a) is attributed primarily to imperfect matching between the different lattice transitions of the linac. The evolution of the RMS and maximum beam envelope is presented in Fig. 4(b). These simulations indicate that the ratio between the minimum beam tube radius and the RMS beam size stays higher than 10 in most of the linac.

## BEAM LOSSES

A detailed study has been performed between TRACK and ASTRA to benchmark the impact of element misalignments and jitter on beam parameters and losses. This work will be reported in Ref. [10]. It has been observed that the major contributor to beam degradation are the transverse rotation and displacement of the solenoids and transverse displace-

Table 2: Typical Set of Errors used for the Simulations of the FNAL 8-GeV Pulsed Linac

Beam Parameter		Error Value	Distribution
Solenoid Displacement (x and y)	[mm]	0.5	Uniform
Solenoid Rotation (x and y)	[mrad]	2	Uniform
Solenoid Field Jitter	[%]	0.5	Gaussian
Quadrupole Displacement (x and y)	[mm]	0.5	Uniform
Quadrupole Rotation (x and y)	[mrad]	2	Uniform
Quadrupole Field Jitter	[%]	0.5	Gaussian
Cavity Displacement (x and y)	[mm]	0.5	Uniform
Cavity Rotation (x and y)	[mrad]	2	Uniform
Cavity Field Jitter	[%]	1.0	Gaussian
Cavity Phase Jitter	[%]	1.0	Gaussian

ment of the quadrupoles.

Typical values of element misalignment and cavity jitter (phase and field) have been implemented into TRACK and ASTRA and beam loss simulations performed from the RFQ exit to the end of the FNAL 8 GeV linac. In order to get high-statistics, 400 simulations were performed on the Fermigrid with a different seed for the random number generator used in each simulation. The simulations were performed with  $5 \times 10^4$  macroparticles and the losses were scaled to a beam power of 2 MW. The set of misalignments and RF errors implemented into the codes is reported in Table 2 and the corresponding beam power loss per meter along the linac in Fig. 5. It is clear from this figure that both codes predict, for the typical set of errors of Table 2, losses along the linac well above the 1 W/m limit. It is also interesting to notice in Fig. 5 that losses tend to be more concentrated in the linac front-end where the beam is most sensitive to the transverse rotation and displacement of the solenoids.

The TRACK correction algorithm, presented in detail in Ref. [11], aims to steer the beam so that the transverse displacements measured by the Beam Position Monitors are minimized. Figure 6(a) shows TRACK simulations of the

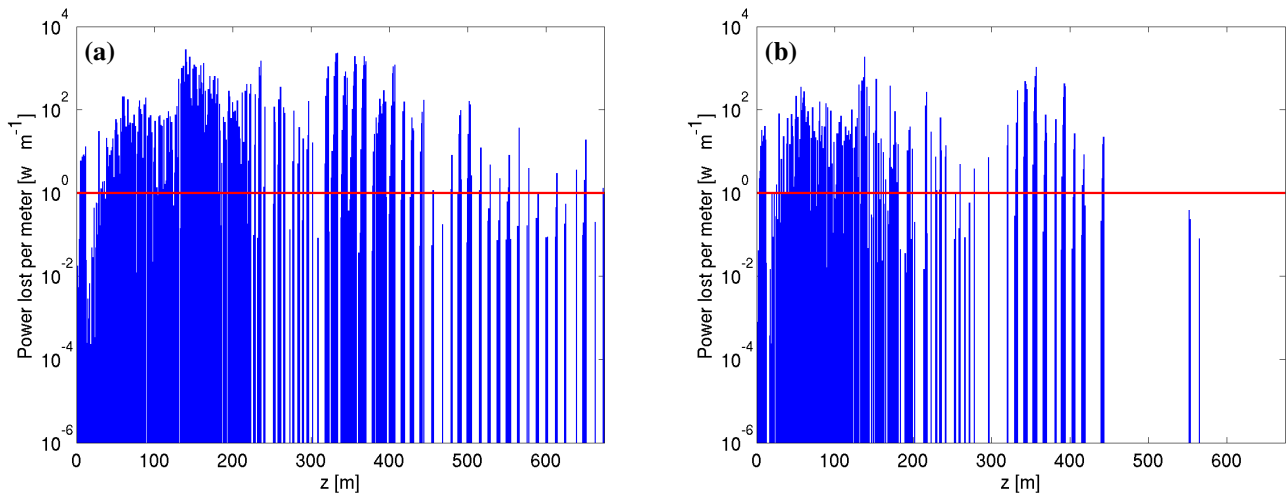


Figure 5: (a) TRACK and (b) ASTRA simulations of the loss pattern along the FNAL 8-GeV pulsed linac operating at 2 MW for the set of errors presented in Table 2. The red bar represents the 1 W/m limit.

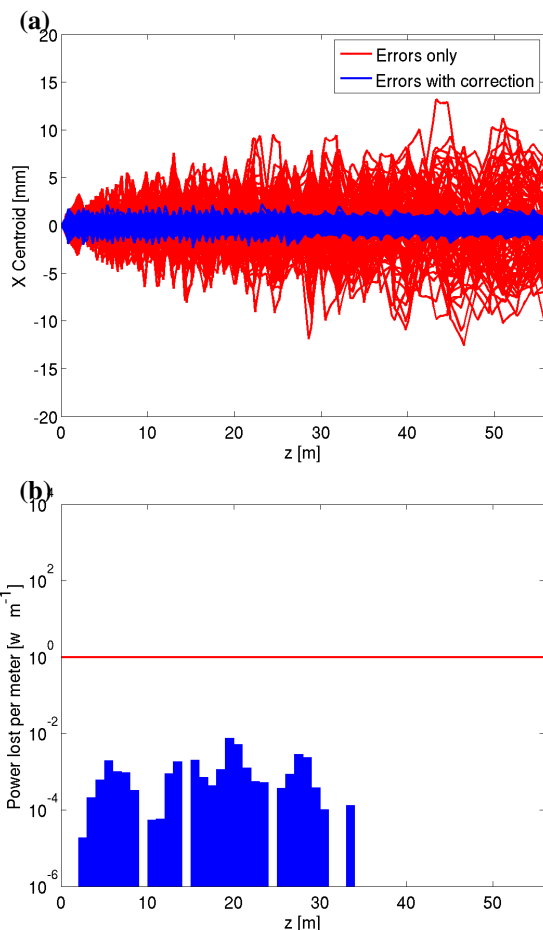


Figure 6: TRACK simulations of (a) corrected / uncorrected beam centroid motion for the front-end (up to  $z \simeq 60$  m) of the FNAL 8-GeV pulsed linac operating at 2 MW for the set of errors presented in Table 2 and using a correction schematic of 1 corrector and 1 monitor per solenoid. (b) corresponding beam loss pattern for the corrected case. The red bar represents the 1 W/m limit.

corrected / uncorrected beam centroid motion for the front-end (up to  $z \simeq 60$  m) of the FNAL 8-GeV pulsed linac operating at 2 MW for the set of errors presented in Table 2 and using a correction schematic of 1 corrector and 1 monitor per solenoid. The resolution and the offset in position of the BPM's are respectively  $30 \mu\text{m}$  and 1 mm. The corresponding beam loss pattern presented in Fig. 6(b) clearly shows the efficiency of the correction schematic, with losses after correction limited to  $< 10^{-2}$  W/m.

### *H<sup>-</sup> Stripping*

A detail study of the stripping effects of the  $\text{H}^-$  ions, namely from blackbody radiation, residual gas and magnetic fields is reported in Ref. [12]. Even though these stripping effects can make serious damage to the  $\text{H}^-$  ions, if proper action is taken their impact can be made marginal.

## CONCLUSION

The considerations used for the design of high-intensity proton and  $\text{H}^-$  linacs have been presented in this paper. As a next step, it would be interesting to benchmark the loss pattern and mechanism of an existing proton driver like SNS with a simulation code to validate our model.

## REFERENCES

- [1] V. N. Aseev *et al.*, TPAT028, PAC'05, 2005.
- [2] [http://www.desy.de/~mpyflo/Astra\\_dokumentation](http://www.desy.de/~mpyflo/Astra_dokumentation)
- [3] S. Peggs, TU203, , LINAC'10.
- [4] CERN-2006-006, (2006).
- [5] S. Henderson, M0103, LINAC'10.
- [6] P. N. Ostroumov, *New J. Phys.* 8, p. 281 (2006).
- [7] N. Solyak, WE101, LINAC'10.
- [8] J. Alonso, FERMIAB-Conf-00/185, (2000).
- [9] J.-P. Carneiro (et al.), NIM A, 606 (2009) 271-280.
- [10] J.-P. Carneiro (et al.), to be submitted to PRST-AB.
- [11] B. Mustapha (et al.), TH6FPF006, PAC'09.
- [12] J.-P. Carneiro (et al.), PRST-AB, 040102, (2009).